

Q-MAMBA: TOWARDS MORE EFFICIENT MAMBA MODELS VIA POST-TRAINING QUANTIZATION

Anonymous authors

Paper under double-blind review

ABSTRACT

State Space Models (SSMs), such as Mamba, have recently demonstrated the potential to match or even surpass Transformers in language understanding tasks, making them a promising alternative for designing Large Language Models (LLMs). Concurrently, model quantization, particularly Post-Training Quantization (PTQ), has been proven effective in reducing memory usage and inference latency in LLMs. In this paper, we explore post-training quantization for Mamba (**Q-Mamba**) by converting both linear projections and state caches into low-bit integers for efficient inference. After a theoretical analysis of the causes of outliers in states, we propose **Decoupled Scale Quantization (DSQ)**, which mitigates outliers in both the state and channel dimensions by applying separate quantization scales. To preserve the selective ability of quantized Mamba, we introduce **Efficient Selectivity Reconstruction (ESR)**, a block-wise reconstruction method that involves a novel quantization simulation scheme, enabling fast parallel scan algorithms with the non-linear quantization function. We demonstrate the effectiveness of Q-Mamba across various quantization settings, model sizes, and both generation and zero-shot tasks. In particular, for Mamba2-2.7B with W8A8H4 quantization, Q-Mamba achieves a 50% reduction in memory consumption with only a 2.13% average accuracy degradation on zero-shot tasks.

1 INTRODUCTION

Large language models (LLMs), such as LLaMa (Touvron et al., 2023) and GPT-4 (OpenAI, 2023), have shown exceptional capabilities in general-purpose language understanding (Kaplan et al., 2020; Hoffmann et al., 2022). However, LLMs based on Transformer architectures still face a significant limitation: the computational cost of their attention mechanism scales quadratically with the sequence length (Vaswani et al., 2017). Therefore, prior works have focused on more efficient attention variants, such as structured state space models (SSMs) (Gu & Dao, 2023; Dao & Gu, 2024; Smith et al., 2023) and linear attention (Peng et al., 2023; Han et al., 2023; Child et al., 2019). Among these, the Mamba architecture (Gu & Dao, 2023; Dao & Gu, 2024) has been shown to match or exceed the downstream accuracy of Transformers on standard language modeling tasks (Waleffe et al., 2024). Following its success in natural language understanding, it has also garnered significant attention in other research areas, such as vision and multimodal tasks (Qiao et al., 2024; Zhu et al., 2024).

Like Transformers, Mamba language models also operate in two computation phases (Patel et al., 2024). The first is the prefill phase, where all input prompt tokens are processed in parallel through the model’s forward pass to generate the first output token. During this phase, Mamba models (Gu & Dao, 2023; Dao & Gu, 2024) employ a hardware-efficient parallel algorithm to compute SSMs (Section 3). The second is the token generation phase, where subsequent output tokens are generated sequentially, relying on the cached state from previous tokens in the sequence. Due to the lack of computational parallelism, this phase tends to be more memory-bound and contributes significantly to the total generation latency.

Although Mamba has successfully replaced the $O(T^2)$ attention module with $O(T)$ selective state space models, our profiling results in Section 4 indicate that it still suffers from two inefficiencies during the generation stage. Firstly, similar to Transformers, the Mamba architecture consists of large linear layers, which require substantial GPU memory and slow down token generation

(Figure 2b). Secondly, as larger states allow more information to be stored, states in Mamba are expanded to be N times larger than vanilla activations, where N is the state dimension (128 in Mamba-2 models). Consequently, these state caches account for a significant portion of memory consumption, especially after quantizing weights to low bits (79.6% in Mamba2-2.7B with a batch size of 128, as shown in Figure 2a). In this paper, we address a key question: *Can Mamba models be further optimized through model compression techniques?*

In this paper, we propose **Q-Mamba**, which quantizes both **linear projections** and **state caches** into low-bit integers for Mamba models. Although previous research has successfully quantized Key and Value (KV) caches into low-bit representations in transformers (Liu et al., 2023; 2024b; Hooper et al., 2024), this work is the first to explore the quantization of state cache in Mamba architectures. We observe that states exhibit both outlier channels and outlier states (i.e., the state dimension contains large values across all channel dimensions), as shown in Figure 3. Further theoretical analysis reveals this phenomenon results from the computation of the outer products of two activations, each of which contains outliers in distinct dimensions. This observation motivates us to propose **Decoupled Scale Quantization (DSQ)**, which utilizes separate quantization scales for both dimensions. Additionally, the non-linear nature of the quantization function disrupts the original equivalence between recurrence and quadratic dual form, the latter being essential for efficient training. To address this, we propose Efficient Selectivity Reconstruction (ESR), which simulates quantization errors by quantizing only the final timestep during training. Specifically, ESR updates a small number of selective parameters (approximately 2% of the total) using just 128 training samples in a block-wise reconstruction manner.

Extensive experiments demonstrate that our methods achieve significant performance improvements for Mamba families on various evaluation metrics. To the best of our knowledge, we are the first to achieve W8A8H4 (8-bit linear projection and 4-bit states) for the Mamba architectures. For generation tasks, Q-Mamba achieved perplexities of 12.99 and 16.90 with 4-bit states on WikiText2 (Merity et al., 2017) and C4 (Pal et al., 2023), respectively, while baseline methods degraded to 21.18 and 29.86 even with 6-bit quantization. Additionally, Q-Mamba achieves W8A8H4 quantization for zero-shot tasks with only 2.13% and 2.11% average accuracy degradation on Mamba2-2.7B and Mamba2-1.3B, respectively.

2 RELATED WORKS

2.1 STATE SPACE MODEL

Transformer-based LLMs (Touvron et al., 2023; OpenAI, 2023) suffer from the computational cost of their attention mechanism scales quadratically with sequence length. Consequently, much research has focused on developing more efficient variants of attention, such as structured state space models (SSMs) (Gu & Dao, 2023; Dao & Gu, 2024; Smith et al., 2023). The original structured SSMs (S4) (Gu et al., 2022) were linear time-invariant (LTI) systems motivated by continuous-time online memorization. Many variants of structured SSMs have been proposed, for example, Gated SSM architectures, such as GSS (Mehta et al., 2023) and BiGS (Wang et al., 2023), incorporate a gating mechanism into SSMs for language modeling. Recently, the Mamba (Gu & Dao, 2023; Dao & Gu, 2024) architecture demonstrates promising performance on standard language modeling tasks (Waleffe et al., 2024), as well as on vision and multimodal tasks (Zhu et al., 2024; Qiao et al., 2024). Mamba showed that state expansion and selective ability are crucial for selecting and memorizing useful information in the hidden states.

2.2 MODEL QUANTIZATION

In the current era of burgeoning LLM development, model quantization has also become widely employed (Xiao et al., 2023; Lin et al., 2023; Frantar et al., 2022). Considering the substantial computational costs of retraining the entire model, much research has focused on Post-Training Quantization (PTQ), which requires only a small amount of calibration data to adjust a limited portion of the parameters. Typically, PTQ methods operate by quantizing and finetuning individual layers or small blocks of consecutive layers. For example, AdaRound (Nagel et al., 2020) uses gradient optimization to determine optimal rounding in a single convolution layer. For LLMs, previous quantization methods have identified significantly larger outliers in activations compared to

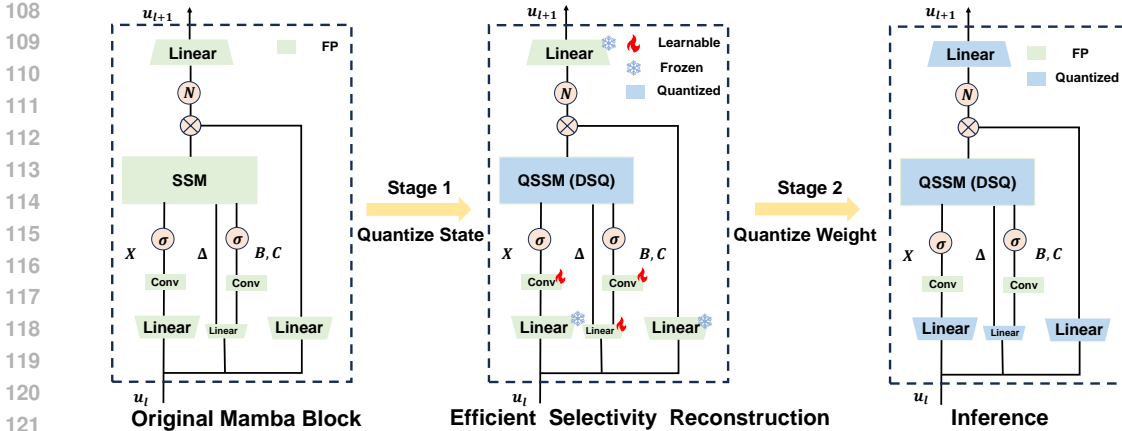


Figure 1: Schematic of the PTQ framework for Mamba. **Left:** The selective parameters B , Δ , and C , along with the SSM inputs x , are generated by the input projections in the Mamba block. **Middle:** After quantizing states using DSQ, ESR updates a small number of selective parameters (approximately 2% of the total) in a block-wise reconstruction manner. **Right:** Finally, we quantize the linear projection into W&A8.

smaller convolutional neural networks (CNNs). To quantize both weights and activations into INT8, SmoothQuant (Xiao et al., 2023) mitigates activation outliers by shifting the quantization difficulty from activations to weights through a mathematically equivalent transformation. These outliers in activations also pose challenges even in scenarios where activations are not quantized (i.e., weight-only quantization) because they amplify the quantization errors of weights when multiplied with activations.

For Mamba models, states have an additional state dimension compared to standard activations, resulting in not only more significant memory consumption but also a distinctive distribution of outliers. To address this issue, we propose two novel methods that enable the quantization of states into 4-bit integers for the first time.

3 FOUNDATIONS

State Space Model. State space models (SSMs) in Equation (1) map a **1-dimensional** input sequence $x_t \in \mathbb{R}$ to an output sequence $y_t \in \mathbb{R}$ through a latent state $h_t \in \mathbb{R}^{(N,1)}$:

$$h_t = \bar{A}h_{t-1} + \bar{B}x_t \quad (1a) \quad h'(t) = Ah(t) + Bx(t) \quad (2a)$$

$$y_t = Ch_t \quad (1b) \quad y(t) = Ch(t) \quad (2b)$$

where $\bar{A} \in \mathbb{R}^{(N,N)}$, $B, \bar{B}, h_{t-1}, h_t, h(t) \in \mathbb{R}^{(N,1)}$, and $C \in \mathbb{R}^{(1,N)}$. Equation (1) can be viewed as discrete versions of a classical continuous system described by Equation (2). Specifically, a timescale parameter Δ is introduced to discretize the parameters A and B into their discrete counterparts, \bar{A} and \bar{B} , as explained in the following sections.

Mamba-1. To operate on an input sequence x_t with D channels, rather than the scalar sequence described earlier, Mamba-1 (Gu & Dao, 2023) assumes that \bar{A} has a diagonal structure and applies the SSM independently to each channel:

$$h_t = \bar{A} \odot h_{t-1} + \bar{B} \odot x_t, \quad \bar{A}, \bar{B}, h_t, h_{t-1} \in \mathbb{R}^{(N,D)}, \quad x_t \in \mathbb{R}^{(1,D)} \quad (3a)$$

$$y_t = Ch_t, \quad C \in \mathbb{R}^{(1,N)}, \quad y_t \in \mathbb{R}^{(1,D)} \quad (3b)$$

where \odot denotes the element-wise product, with automatic broadcasting applied to dimensions of size one.. The discretized parameters are defined as $\bar{A} = \exp(A \odot \Delta)$ and $\bar{B} = B \odot \Delta$, where $A \in \mathbb{R}^{(N,D)}$, $B \in \mathbb{R}^{(N,1)}$, and $\Delta \in \mathbb{R}^{(1,D)}$. Unlike previous non-selective SSMs, Mamba set Δ , B , and C as functions of the inputs rather than fixed parameters. As a result, the variables \bar{A} , \bar{B} , and C can vary across time steps to dynamically select relevant information from the context.

Mamba-2. To integrate the multi-head design of modern attention mechanisms into Mamba architectures, Mamba-2 (Dao & Gu, 2024) further assumes that \bar{A} and \bar{B} are identical across all dimensions **within the same head** where the head dimension $P \in \{64, 128\}$:

$$h_t = \bar{A} \cdot h_{t-1} + \bar{B} \otimes x_t, \quad h_t, h_{t-1} \in \mathbb{R}^{(N,P)}, \quad \bar{A} \in \mathbb{R}, \quad \bar{B} \in \mathbb{R}^{(N,1)} \quad (4a)$$

$$y_t = Ch_t, \quad C \in \mathbb{R}^{(1,N)}, \quad x_t, y_t \in \mathbb{R}^{(1,P)} \quad (4b)$$

The discretized parameters are still defined as $\bar{A} = \exp(A \odot \Delta)$ and $\bar{B} = B \odot \Delta$. However, unlike Mamba-1, A and Δ are simplified into two scalars within a single head, transforming the operation between \bar{B} and x into an outer product. This simplification improves training efficiency and allows for a larger state size. Consequently, Mamba-2 increases the state size N from 16 in Mamba-1 to 128. Figure 1 left shows the architecture of the Mamba-2 block. The selective parameters B , Δ , and C , along with the SSM inputs x_t , are produced by the input projections in the Mamba block. Specifically, Mamba-2 employs $B = (uW_B)^\top$, $C = uW_C$, $\Delta = uW_\Delta$, $x_t = uW_x$, where $W_B, W_C \in \mathbb{R}^{(D,N)}$, $W_x \in \mathbb{R}^{(D,P)}$, $W_\Delta \in \mathbb{R}^{(D,1)}$ and $u \in \mathbb{R}^{(1,D)}$ represents the inputs of Mamba block.

Parallel Training. The recurrent mode described in Equation (1) is used only during the token generation phase, where output tokens are generated sequentially, relying on the cached state from the previous timestep. For parallel training, Mamba Dao & Gu (2024) establishes the **equivalence** between selective SSMs and semiseparable matrices, enabling the use of efficient algorithms for structured matrix multiplication (e.g. prefix sum algorithm (Goldberg & Zwick, 1995)). Specifically, Equation (5) represents the **quadratic form** of Equation (1) to compute all timesteps simultaneously:

$$y_t = \sum_{s=0}^t C_t \bar{A}_{t:s}^\times B_s x_s, \quad \bar{B}, \bar{C}^\top \in \mathbb{R}^{(N,1)}, \quad \bar{A} \in \mathbb{R}^{(N,N)}, \quad x_t, y_t \in \mathbb{R} \quad (5)$$

$$y = Mx, \quad M_{ji} := C_j A_j \cdots A_{i+1} B_i, \quad M \in \mathbb{R}^{(T,T)}$$

where M is N-semiseparable matrix.

This paper primarily focuses on quantizing the Mamba-2 architecture, which has demonstrated superior performance compared to Mamba-1 across various tasks (Waleffe et al., 2024; Dao & Gu, 2024). A detailed comparison between the two architectures from a quantization perspective is provided in the appendix. For more information on the Mamba architecture, please refer to the original papers (Gu & Dao, 2023; Dao & Gu, 2024).

4 ANALYSIS

In this section, we first analyze the memory consumption and runtime of primary components on the Mamba2-2.7B model, i.e., linear projection, 1D convolution, SSM, and LayerNorm. Based on the results presented in Figures 2a and Figures 2b, we can draw the following conclusions:

Linear projections. Similar to Transformers, large linear layers in Mamba not only require substantial GPU memory but also slow down token generation. When applying quantization to these linear layers, experiments in Section A.1 reveal that outliers exist in specific activation channels of Mamba, particularly in output projections. This phenomenon has also been observed in previous studies on Transformer-based LLMs (Xiao et al., 2023; Wei et al., 2022).

States in SSMs. As larger states allow more information to be stored, states in Mamba are expanded to be N times larger than vanilla activations, where N is the state dimension (128 in Mamba-2 models). Consequently, these state caches account for a significant portion of memory consumption, especially after quantizing weights to low bits (e.g., 79.6% in Mamba2-2.7B with a batch size of 128, as shown in Figure 2a). This phenomenon not only poses challenges for increasing the batch size to enhance throughput but also prevents further enlargement of state dimensions in Mamba models, which would improve their storage capacity for long contexts (Dao & Gu, 2024; Arora et al., 2024).

To address the above problems, in this paper, we aim to quantize both linear projections and state caches into low-bit integers for Mamba models.

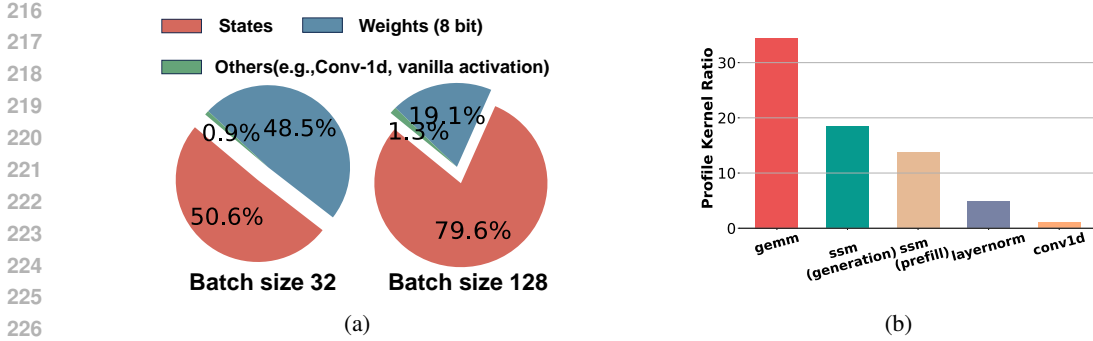


Figure 2: State distribution in Mamba2-370M. **Left:** Memory consumption of weights and state caches in Mamba2-2.7B with different batch sizes. **Right:** The Runtime of the Mamba2-2.7B model using NVIDIA profiling tools, with both prompt and generation lengths set to 100 and a batch size of 32.

5 METHOD

5.1 DECOUPLED SCALE QUANTIZATION

5.1.1 OUTLIERS IN STATES

For Transformers, particularly LLMs, extensive research (Wei et al., 2022; Xiao et al., 2023; Liu et al., 2024a) has shown that the presence of outliers extends the range of activation values, which in turn increases quantization errors for normal values. In Mamba models, we observe a similar or even more pronounced issue with outliers in the states. As illustrated in the state distribution visualization in Figure 3(a), outliers are present in both state dimensions (red row) and channel dimensions (green column). Consequently, either per-channel quantization (i.e., using a different quantization step for each channel) or per-state quantization (i.e., using a different quantization step for each state) tends to ignore outliers in the other dimension. As shown in Table 3, the model’s performance declines significantly when adopting the above quantization granularity, which calls for a more effective quantization method to address the problem.

5.1.2 DECOUPLED SCALE QUANTIZATION

Motivated by the distribution characteristics shown in Figure 3, we present the following theorem, which reveals the underlying causes of this distribution and provides insights for a solution.

Theorem 1. Assuming $u_t \sim \mathcal{N}(\mathbf{0}, \sigma \mathbf{I}_n)$ and A_t is a constant, $B_t = (uW_B)^\top$, $x_t = uW_x$, the variance of states $h_t = A_t \cdot h_{t-1} + B_t \otimes x_t$ can be factorized into two vectors:

$$\text{Var}[h_t] \propto \alpha \cdot \beta^T, \quad \alpha_i = \|W_{i,:}^x\|_2^2 \quad \text{and} \quad \beta_i = \|W_{i,:}^B\|_2^2 \quad (6)$$

The above theorem demonstrates that outliers in the channel dimension P and state dimension N can be attributed to variables x_t and B_t , respectively. A visualization of this phenomenon is provided in Figure 3(b). This motivates us to propose a novel quantization scheme called **Decoupled Scale Quantization (DSQ)**, which utilizes separate quantization scales for the state dimension and the channel dimension:

$$\mathbf{H} = \mathbf{S}_{state} \times \hat{\mathbf{H}} \times \mathbf{S}_{channel}$$

0.5	2.0	2.0	1.5
9.0	18	54	9.0
6.0	4.0	8.0	2.0
2.0	8.0	16	6.0

$$\mathbf{S}_{channel} = \sqrt{\text{mean}(|\mathbf{H}_{i,:}|)}$$

0.5
1.5
1.0
1.0

$$\hat{\mathbf{H}} = \begin{bmatrix} 1 & 2 & 1 & 3 \\ 6 & 6 & 9 & 6 \\ 6 & 2 & 2 & 2 \\ 2 & 4 & 4 & 6 \end{bmatrix}$$

$$\mathbf{S}_{state} = \max(|\mathbf{H}_{i,:}|/S_{channel})$$

1.0	2.0	4.0	1.0
-----	-----	-----	-----

Figure 4: An illustration of DSQ.

$$Q(h) = \lfloor \frac{h}{S_{channel} \cdot S_{state}^\top} \rfloor \odot (S_{channel} \cdot S_{state}^\top) \quad (7)$$

where $S_{channel} \in \mathbb{R}^P$, $S_{state} \in \mathbb{R}^N$ and $\lfloor \cdot \rfloor$ denotes rounding floating-point values to the nearest integers, while \odot signifies element-wise multiplication.

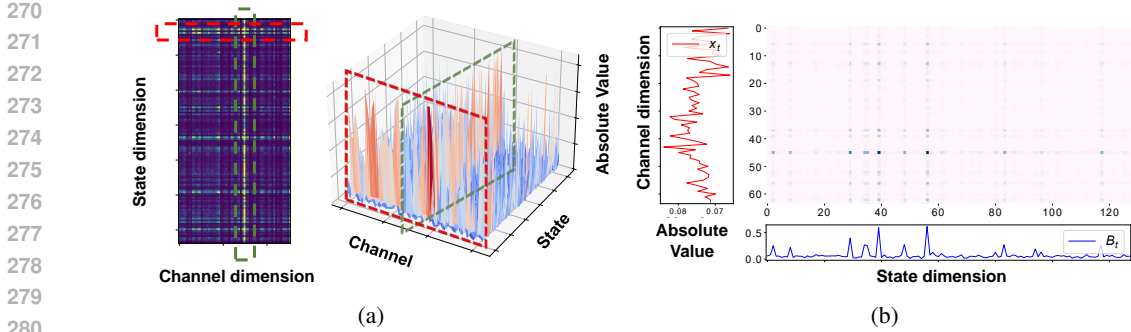


Figure 3: State distribution in Mamba2-370M. **Left:** Outliers exist in both specific state dimensions (red) and channel dimensions (green). **Right:** Further analysis reveals outliers in channel dimension and state dimension can be attributed to variables x_t and B_t , respectively.

In this paragraph, we discuss how to compute scales given a specific state. To increase the effective quantization bits, both state and channel scales should accurately represent the magnitude of their respective dimensions. Therefore, an intuitive metric to determine these scales is the vector norm, such as maximum norm ($\|\cdot\|_\infty$) and L^1 norm ($\|\cdot\|_1$). However, in practice, we find that both norms result in even worse performance (see Table 5). Further visualization in Figure 8 shows that these norms are highly sensitive to outliers, resulting in even greater bit wastage. Therefore, for the channel scale, we use the square root of the mean values, which offers a more robust metric that mitigates the influence of outliers. After mitigating most outliers by smoothing the states with channel scale, we employ the MinMax method to compute state scale, which effectively compresses the data range and reduces information loss during quantization:

$$S_{channel,i} = \text{sqrt}(\text{mean}(\text{abs}(h_{i,:}))) = \sqrt{\|h_{i,:}\|_1} \quad (8)$$

$$S_{state,j} = \max(\text{abs}(\frac{h_{:,j}}{S_{channel}})) = \|\frac{h_{:,j}}{S_{channel}}\|_\infty \quad (9)$$

where i and j denote subscripts indexing into the channel and state dimensions, respectively. Table 3 demonstrates that DSQ achieves negligible overhead while significantly improving performance.

5.2 EFFICIENT SELECTIVITY RECONSTRUCTION

To mitigate the performance loss caused by quantization, PTQ methods often apply block-wise reconstruction (Nagel et al., 2020; Li et al., 2021) with a few data. However, these methods cannot be directly applied to Mamba models due to the following differences: First, when applying the non-linear quantization function to states h_t , the definition of SSMs can no longer be reformulated into quadratic mode for parallel training. Second, given the distinct mechanisms between Mamba and Transformers, it is necessary to investigate which set of parameters is critical for restoring model performance and which may lead to overfitting. In this section, we will present **Efficient Selectivity Reconstruction** (ESR) with the mechanisms to address these two challenges in Section 5.2.1 and Section 5.2.2, respectively.

5.2.1 QUANTIZATION-AWARE STATE SPACE MODEL

To minimize memory bandwidth utilization, we store state caches as low-bit elements, then load and dequantize them before computation at the next timestep. This process defines a new sequence transformation through the quantized latent state h_t^q in Equation (10). It is important to distinguish $h_t^q = \bar{A}Q(h_{t-1}^q) + \bar{B}x_t$ from the quantized value of the original h_t , denoted as $Q(h_t)$, where the latter is given by $Q(h_t) = Q(\bar{A}h_{t-1} + \bar{B}x_t)$.

$$h_t^q = \bar{A}Q(h_{t-1}^q) + \bar{B}x_t, \quad (10a)$$

$$y_t^q = Ch_t^q \quad (10b)$$

A significant challenge arises because the original parallel training algorithms are incompatible with the quantization scenario. Specifically, the non-linear nature of the quantization function breaks the equivalence between the recurrent and quadratic modes. (In other words, this equivalence relies on the linearity of original SSMs.) A naive approach would involve directly applying Equation (10) for token-by-token generation. However, given the large input lengths (e.g., 2048), this method is extremely slow and impractical. Therefore, to apply block-wise reconstruction for Mamba models, it is essential to first investigate how to effectively simulate quantization errors during training.

$$\begin{aligned} h_t^q &= \bar{A}_t Q(h_{t-1}^q) + \bar{B}_t x_t \\ &= \bar{A}_t Q(\bar{A}_{t-1} h_{t-2}^q + \bar{B}_{t-1} x_{t-1}) + \bar{B}_t x_t \\ &\neq \bar{A}_t \bar{A}_{t-1} Q(h_{t-2}^q) + \bar{A}_t \bar{B}_{t-1} x_{t-1} + \bar{B}_t x_t \\ &\neq \sum_{s=1}^t \bar{A}_s \bar{A}_{s+1} \cdots \bar{A}_t \bar{B}_s x_s \end{aligned} \quad (11)$$

To gain insight into this problem, we focus on the difference between the quantized and original states, which is defined as $\delta_t = h_t^q - h_t$. By substituting δ_t into Equation (10), we observe that δ_t is composed of two parts: the quantization error propagated from the previous timestep, δ_{t-1} , and the quantization error introduced in the current timestep:

$$\begin{aligned} \delta_t &= h_t^q - h_t = \bar{A}_t Q(h_{t-1}^q) + \bar{B}_t x_t - (\bar{A}_t h_{t-1} + \bar{B}_t x_t) \\ &= \bar{A}_t \cdot (Q(h_{t-1}^q) - h_{t-1}) \\ &= \bar{A}_t \cdot (Q(h_{t-1} + \delta_{t-1}) - h_{t-1}) \end{aligned} \quad (12)$$

Assuming that quantization errors δ_{t-1} are sufficiently small compared to the hidden state h_{t-1} , we discard δ_{t-1} and focus only on the quantization errors at the current timestep:

$$\begin{aligned} Q(h_{t-1} + \delta_{t-1}) &\approx Q(h_{t-1}) + Q'(h_{t-1}) \cdot \delta_{t-1} \approx Q(h_{t-1}) \\ \implies h_t^q &\approx \bar{A}_t Q(h_{t-1}) + \bar{B}_t x_t \end{aligned} \quad (13)$$

Equation (13) enables us to utilize the parallel algorithm to compute h_t at all timesteps, then simulate the quantization errors by quantizing only one step during training. In the appendix, we present the pseudocode for the parallel training of quantization-aware SSMs for illustrative purposes. Table 4 demonstrates the effectiveness of this quantization simulation, especially in low-bit settings.

5.2.2 SELECTIVITY GUIDED ADAPTATION

In the Mamba block, the selective parameters B , Δ , and C , along with the SSM inputs x_t , are generated through input projections, as shown in Figure 1. During block-wise reconstruction, we freeze the linear projections corresponding to the SSM inputs x and z , while keeping the linear projections for selective parameters B , C , and Δ learnable, which is referred to as Selectivity Guided Adaptation (SGA) (Figure 1, middle). Specifically,

$$\min_{\{W_v^q | v \in B, C, \Delta\}} \|\mathcal{B}_l(W_v^{FP}, h_t^{FP}; u_l) - \mathcal{B}_l(W_v^q, h_t^q; u_l)\|_2, \quad v \in \{x, z, B, C, \Delta\} \quad (14)$$

where \mathcal{B}_l denotes the $-th$ mapping function for the l -th Mamba block and u_l represents the block’s inputs. W^{FP} and W^q represent the weights of the original model and the quantized model, respectively.

SGA offers two primary advantages: First, the success of Mamba is largely attributed to the selectivity of parameters \bar{A} , \bar{B} , and \bar{C} , which distinguishes it from earlier non-selective SSMs (Gu et al., 2020; Smith et al., 2023). Thus, we hypothesize that this selectivity also plays a critical role in maintaining performance after quantization. Second, SGA reduces the number of learnable parameters, mitigating the risk of overfitting with limited calibration data. For example, in Mamba2-2.7B, learnable parameters account for only about 2% of the total. Note that during this fine-tuning process, the linear layers remain in floating-point values and can be quantized afterward (Figure 1, right).

Table 1: Evaluation results of the Mamba-2 models on generation tasks. #W, #A, and #H indicate weight bits, activation bits, and state bits, respectively.

Bits	Method	WikiText2 ↓					C4 ↓				
		130M	370M	780M	1.3B	2.7B	130M	350M	780M	1.3B	2.7B
FP16	-	20.04	14.16	11.81	10.42	9.06	22.25	16.95	14.66	13.27	11.95
W16A16H4	Baseline	976.56	913.34	865.78	1556.15	116.23	542.048	599.49	911.31	529.55	96.93
	Q-Mamba	45.73	22.24	19.07	15.20	11.55	39.46	26.36	22.45	19.14	14.90
W16A16H6	Baseline	249.09	134.91	38.04	23.62	13.60	322.97	101.75	38.24	23.73	19.61
	Q-Mamba	23.79	15.33	12.69	11.37	9.59	25.11	18.27	15.66	14.52	12.57
W16A16H8	Baseline	20.97	14.83	12.04	10.52	9.11	22.97	17.45	14.85	13.40	12.01
	Q-Mamba	20.49	14.26	11.86	10.51	9.11	22.64	17.05	14.73	13.39	12.04
W8A8H4	Baseline	2024.49	1013.15	7225.39	6375.57	364.84	635.86	795.28	10716.17	2788.23	298.57
	Q-Mamba	53.12	27.53	23.53	17.60	12.99	46.90	32.91	26.79	21.56	16.90
W8A8H6	Baseline	357.69	220.09	96.51	47.28	21.18	526.59	171.90	79.70	40.46	29.86
	Q-Mamba	26.75	17.27	14.51	13.05	10.84	28.18	20.53	17.79	16.45	14.46
W8A8H8	Baseline	23.60	16.69	14.32	11.85	10.42	25.51	19.50	17.44	14.86	13.73
	Q-Mamba	22.88	15.83	13.57	11.93	10.36	25.01	18.84	16.80	15.03	13.69

6 EXPERIMENTS

6.1 EXPERIMENT SETUP

Settings. We conduct experiments on the Mamba-2 (Dao & Gu, 2024) models across various model sizes (130M, 370M, 780M, 1.3B, 2.7B). We initialize quantized models using a full-precision model. We utilize the AdamW optimizer with zero weight decay to optimize the learnable parameters in ESR. The learning rate for learnable parameters is set to $1e-3$. RedPajama is an open-source reproduction of the pre-training data for LLaMA (Touvron et al., 2023). We employ a calibration dataset consisting of 128 randomly selected 2048-token segments from the RedPajama (Computer, 2023) dataset, except for Mamba2-2.7B, which utilizes 256 samples. The entire training process is facilitated on a single NVIDIA A800 GPU, using a batch size of 1 over 3 epochs. For linear projections, we apply SmoothQuant (Xiao et al., 2023) with per-token quantization. For state quantization, we use INT8, INT6, and INT4 schemes (e.g., W8A8H4 refers to 8-bit linear projection and 4-bit quantization of the states). We utilize MinMax per-channel quantization (introduced in Section 5.1.2) as state quantization **baseline**.

Evaluation Tasks. We evaluate our methods on both language generation and zero-shot tasks. We report the perplexity on WikiText2 (Merity et al., 2017) and C4 (Pal et al., 2023). For zero-shot tasks, we provide accuracy on datasets including PIQA (Bisk et al., 2020), ARC (Clark et al., 2018), BoolQ (Clark et al., 2019), OpenBookQA (Mihaylov et al., 2018), HellaSwag (Zellers et al., 2019) and Winogrande (Sakaguchi et al., 2020).

6.2 MAIN RESULTS

Generation Tasks. We evaluate generation tasks in recurrent mode with a sequence length of 2048. The results in Table 1 demonstrate the effectiveness of Q-Mamba across various quantization configurations. For INT8 state quantization, we exclusively utilize DSQ without ESR, as DSQ alone achieves nearly lossless quantization compared to full-precision models. Without our methods, states are limited to 8-bit quantization, with lower-bit quantization, such as 6-bit, leading to significant performance degradation, e.g., 23.62 perplexity for Mamba2-1.3B on the WikiText2 dataset. In contrast, Q-Mamba facilitates nearly lossless 6-bit quantization, achieving a minimal degradation of only 0.53 perplexity for Mamba2-2.7B and 0.88 perplexity for Mamba2-1.3B. Moreover, Q-Mamba enables effective 4-bit quantization and is compatible with the linear projection quantization approach. For example, Q-Mamba achieves 12.99 perplexity in W8A8H4 quantization settings for the Mamba2-2.7B model.

Zero-shot Tasks. We evaluate the performance of Q-Mamba on zero-shot tasks using the lm-eval-harness (Gao et al., 2024) framework in Table 2. Q-Mamba significantly improves the average accuracy across various models. For example, it increases the average accuracy by 6.37%, 6.55%,

Table 2: Evaluation results of the Mamba-2 models with W8A8H4 (8-bit weights, activations, and 4-bit states) on zero-shot tasks.

Model	Method	OBQA	PIQA	ARC-E	ARC-C	HellaSwag	WINO	AVG \uparrow
Mamba2-130M	FP	30.6	64.9	47.4	24.2	35.3	52.1	42.41
	Baseline	30.8	63.4	45.6	24.6	34.1	51.93	41.73
	Q-Mamba	30.0	63.0	45.7	23.4	33.9	53.3	41.55
Mamba2-370M	FP	32.4	70.5	54.9	26.9	46.9	55.7	47.83
	Baseline	28.6	58.6	46.5	24.9	30.4	53.0	40.34
	Q-Mamba	32.8	68.4	53.8	26.7	43.8	54.8	46.71
Mamba2-780M	FP	36.2	72.0	61.0	28.5	54.9	60.2	52.13
	Baseline	32.0	61.8	50.5	25.9	29.5	57.5	42.85
	Q-Mamba	34.2	69.6	57.3	27.6	52.1	55.6	49.4
Mamba2-1.3B	FP	37.8	73.2	64.3	33.3	59.9	60.9	54.9
	Baseline	35.6	67.1	57.6	29.2	36.8	58.5	47.46
	Q-Mamba	34.8	72.6	62.5	31.4	55.7	59.5	52.77
Mamba2-2.7B	FP	38.8	76.4	69.6	36.4	66.6	64.0	58.63
	Baseline	39.8	73.2	66.8	36.0	56.4	59.6	55.30
	Q-Mamba	40.0	73.9	66.8	35.4	62.0	61.0	56.52

and 5.31% on the 370M, 780M, and 1.3B models. Additionally, for Mamba2-2.7B and Mamba2-1.3B, Q-Mamba achieves W8A8H4 quantization with only 2.13% and 2.11% accuracy degradation.

Table 3: The performance and overheads of different quantization methods on Mamba2-370M. P and N denote channel and state dimensions, respectively.

Granularity	WikiText2 \downarrow	Overheads
Per-tensor	4815.83	$\frac{1}{P \times N}$
Per-channel	3364.58	$\frac{1}{P}$
Per-state	947.88	$\frac{1}{N}$
DSQ	25.73	$\frac{1}{P} + \frac{1}{N}$

Table 4: Efficacy of each component in ESR. ESR enables adjusting parameters of Mamba blocks after quantizing states **in block-wise reconstruction**. When combined with SGA, these two techniques further enhance performance.

Method	WikiText2 \downarrow	C4 \downarrow
DSQ w/o ESR	25.73	29.94
DSQ+ESR (w/o SGA)	23.73	28.19
DSQ+ESR (w/ SGA)	21.92	25.99

6.3 ABLATIONS

In this section, we conduct experiments to validate the efficacy of each component, as well as the design choices for DSQ, training epochs, and calibration data size. In Section A.3 of the Appendix, we provide visualizations of DSQ and a detailed analysis of the impact of trainable parameters in ESR.

Effectiveness of each component. Table 3 demonstrates that DSQ is essential in state quantization. The model’s performance declines significantly when per-channel or per-state quantization methods are adopted. By decoupling scales in the state and channel dimensions, DSQ mitigates outliers in both dimensions with negligible overhead. Table 4 shows that we can further enhance model performance in block-wise reconstruction with ESR. Furthermore, finetuning selective parameters instead of all parameters can help avoid overfitting and yield better results.

Design choices of DSQ. The results in Table 5 highlight the critical importance of selecting appropriate quantization scales for DSQ. Firstly, squaring the norms as quantization scales is essential for maintaining stability. Furthermore, using mean values yields superior performance compared to relying on maximum values.

Samples and epochs for block-wise reconstruction. To ensure training efficiency, we set 3 epochs and 128 samples for all experiments, except for Mamba2-2.7B, where we use 256 samples. How-

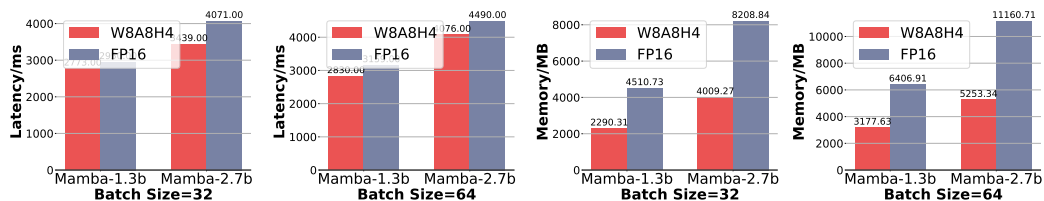


Figure 5: Inference latency and memory usage of the Mamba2 models with different batch sizes on NVIDIA GeForce RTX 3090.

ever, as shown in Figure 6, performance can be further improved by increasing the number of training samples and epochs.

6.4 EFFICIENCY

Figure 5 presents the memory and time requirements for inference using Mamba2 models. For W8A8 linear projections, we employ CUDA INT8 GEMM, following the approach of SmoothQuant (Xiao et al., 2023). For INT4 state quantization, we implement SSM kernels with quantized and packed states with Triton (Tillet et al., 2019), a language and compiler for CUDA computation. Both the input context and generation length are set to 100. The results show that the quantized models can reduce memory usage by half while maintaining or even improving inference latency.

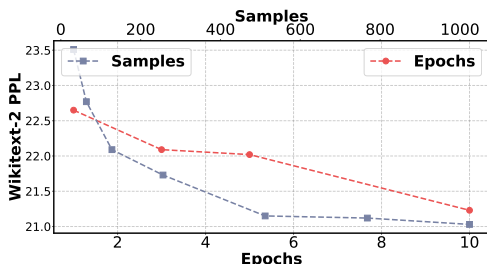


Figure 6: Illustration of WikiText2 perplexity of W16A16H4 quantization with different training samples and epochs.

Table 5: Impact of different design choices for DSQ. Experiments are conducted on Mamba2-370M with W16A16H4 quantization.

Method	WikiText2 ↓	C4 ↓
abs.max	inf	inf
abs.max.sqrt	42.88	46.61
abs.mean	inf	inf
abs.mean.sqrt	25.73	29.94

7 CONCLUSION

In this paper, we propose Q-Mamba, a novel quantization scheme designed for Mamba models. After visualizing outliers in states, we conduct a theoretical analysis of their causes and propose Decoupled Scale Quantization (DSQ). By decoupling scales in the state and channel dimensions, DSQ mitigates outliers in both dimensions while introducing negligible overhead. To further boost performance through block-wise reconstruction, we propose Efficient Selectivity Reconstruction (ESR), which includes a novel quantization simulation method that enables efficient fine-tuning of selective parameters with parallel scan mode. We validate the performance of Q-Mamba across various quantization settings, model sizes, and both generation and zero-shot tasks. In conclusion, Q-Mamba demonstrates that Mamba architectures have the potential for further optimization when combined with other model compression techniques.

REFERENCES

Simran Arora, Sabri Eyuboglu, Michael Zhang, Aman Timalsina, Silas Alberti, Dylan Zinsley, James Zou, Atri Rudra, and Christopher Ré. Simple linear attention language models balance the recall-throughput tradeoff. *CoRR*, abs/2402.18668, 2024. doi: 10.48550/ARXIV.2402.18668. URL <https://doi.org/10.48550/arXiv.2402.18668>.

- 540 Yonatan Bisk, Rowan Zellers, Ronan Le Bras, Jianfeng Gao, and Yejin Choi. PIQA: reasoning
541 about physical commonsense in natural language. In *The Thirty-Fourth AAAI Conference on*
542 *Artificial Intelligence, AAAI 2020, The Thirty-Second Innovative Applications of Artificial Intel-*
543 *ligence Conference, IAAI 2020, The Tenth AAAI Symposium on Educational Advances in Artifi-*
544 *cial Intelligence, EAAI 2020, New York, NY, USA, February 7-12, 2020*, pp. 7432–7439. AAAI
545 Press, 2020. doi: 10.1609/AAAI.V34I05.6239. URL <https://doi.org/10.1609/aaai.v34i05.6239>.
- 547 Rewon Child, Scott Gray, Alec Radford, and Ilya Sutskever. Generating long sequences with sparse
548 transformers. URL <https://openai.com/blog/sparse-transformers>, 2019.
- 550 Christopher Clark, Kenton Lee, Ming-Wei Chang, Tom Kwiatkowski, Michael Collins, and Kristina
551 Toutanova. Boolq: Exploring the surprising difficulty of natural yes/no questions. In Jill Burstein,
552 Christy Doran, and Thamar Solorio (eds.), *Proceedings of the 2019 Conference of the North Amer-*
553 *ican Chapter of the Association for Computational Linguistics: Human Language Technologies,*
554 *NAACL-HLT 2019, Minneapolis, MN, USA, June 2-7, 2019, Volume 1 (Long and Short Papers)*,
555 pp. 2924–2936. Association for Computational Linguistics, 2019. doi: 10.18653/V1/N19-1300.
556 URL <https://doi.org/10.18653/v1/n19-1300>.
- 557 Peter Clark, Isaac Cowhey, Oren Etzioni, Tushar Khot, Ashish Sabharwal, Carissa Schoenick, and
558 Oyvind Tafjord. Think you have solved question answering? try arc, the AI2 reasoning challenge.
559 *CoRR*, abs/1803.05457, 2018. URL <http://arxiv.org/abs/1803.05457>.
- 560 Together Computer. Redpajama: an open dataset for training large language models, 2023. URL
561 <https://github.com/togethercomputer/RedPajama-Data>.
- 562 Tri Dao and Albert Gu. Transformers are ssms: Generalized models and efficient algorithms through
563 structured state space duality, 2024.
- 564 Elias Frantar, Saleh Ashkboos, Torsten Hoefler, and Dan Alistarh. GPTQ: accurate post-training
565 quantization for generative pre-trained transformers. *CoRR*, abs/2210.17323, 2022. doi: 10.
566 48550/ARXIV.2210.17323. URL <https://doi.org/10.48550/arXiv.2210.17323>.
- 567 Leo Gao, Jonathan Tow, Baber Abbasi, Stella Biderman, Sid Black, Anthony DiPofi, Charles Fos-
568 ter, Laurence Golding, Jeffrey Hsu, Alain Le Noac’h, Haonan Li, Kyle McDonell, Niklas Muen-
569 nighoff, Chris Ociepa, Jason Phang, Laria Reynolds, Hailey Schoelkopf, Aviya Skowron, Lin-
570 tang Sutawika, Eric Tang, Anish Thite, Ben Wang, Kevin Wang, and Andy Zou. A framework
571 for few-shot language model evaluation, 07 2024. URL <https://zenodo.org/records/12608602>.
- 572 Tal Goldberg and Uri Zwick. Optimal deterministic approximate parallel prefix sums and their appli-
573 cations. In *Third Israel Symposium on Theory of Computing and Systems, ISTCS 1995, Tel Aviv,*
574 *Israel, January 4-6, 1995, Proceedings*, pp. 220–228. IEEE Computer Society, 1995. doi: 10.
575 1109/ISTCS.1995.377028. URL <https://doi.org/10.1109/ISTCS.1995.377028>.
- 576 Albert Gu and Tri Dao. Mamba: Linear-time sequence modeling with selective state spaces. *CoRR*,
577 abs/2312.00752, 2023. doi: 10.48550/ARXIV.2312.00752. URL <https://doi.org/10.48550/arXiv.2312.00752>.
- 578 Albert Gu, Tri Dao, Stefano Ermon, Atri Rudra, and Christopher Ré. Hippo: Recurrent memory
579 with optimal polynomial projections. In Hugo Larochelle, Marc’Aurelio Ranzato, Raia Had-
580 sell, Maria-Florina Balcan, and Hsuan-Tien Lin (eds.), *Advances in Neural Information Process-*
581 *ing Systems 33: Annual Conference on Neural Information Processing Systems 2020, NeurIPS*
582 *2020, December 6-12, 2020, virtual*, 2020. URL [https://proceedings.neurips.cc/](https://proceedings.neurips.cc/paper/2020/hash/102f0bb6efb3a6128a3c750dd16729be-Abstract.html)
583 [paper/2020/hash/102f0bb6efb3a6128a3c750dd16729be-Abstract.html](https://proceedings.neurips.cc/paper/2020/hash/102f0bb6efb3a6128a3c750dd16729be-Abstract.html).
- 584 Albert Gu, Karan Goel, and Christopher Ré. Efficiently modeling long sequences with structured
585 state spaces. In *The Tenth International Conference on Learning Representations, ICLR 2022,*
586 *Virtual Event, April 25-29, 2022*. OpenReview.net, 2022. URL [https://openreview.net/](https://openreview.net/forum?id=uYLFoz1v1AC)
587 [forum?id=uYLFoz1v1AC](https://openreview.net/forum?id=uYLFoz1v1AC).

- 594 Dongchen Han, Tianzhu Ye, Yizeng Han, Zhuofan Xia, Shiji Song, and Gao Huang. Agent attention:
595 On the integration of softmax and linear attention. *CoRR*, abs/2312.08874, 2023. doi: 10.48550/
596 ARXIV.2312.08874. URL <https://doi.org/10.48550/arXiv.2312.08874>.
597
- 598 Jordan Hoffmann, Sebastian Borgeaud, Arthur Mensch, Elena Buchatskaya, Trevor Cai, Eliza
599 Rutherford, Diego de Las Casas, Lisa Anne Hendricks, Johannes Welbl, Aidan Clark, Tom Hen-
600 nigan, Eric Noland, Katie Millican, George van den Driessche, Bogdan Damoc, Aurelia Guy,
601 Simon Osindero, Karen Simonyan, Erich Elsen, Jack W. Rae, Oriol Vinyals, and Laurent Sifre.
602 Training compute-optimal large language models. *CoRR*, abs/2203.15556, 2022. doi: 10.48550/
603 ARXIV.2203.15556. URL <https://doi.org/10.48550/arXiv.2203.15556>.
- 604 Coleman Hooper, Sehoon Kim, Hiva Mohammadzadeh, Michael W. Mahoney, Yakun Sophia Shao,
605 Kurt Keutzer, and Amir Gholami. Kvquant: Towards 10 million context length LLM inference
606 with KV cache quantization. *CoRR*, abs/2401.18079, 2024. doi: 10.48550/ARXIV.2401.18079.
607 URL <https://doi.org/10.48550/arXiv.2401.18079>.
- 608 Jared Kaplan, Sam McCandlish, Tom Henighan, Tom B. Brown, Benjamin Chess, Rewon Child,
609 Scott Gray, Alec Radford, Jeffrey Wu, and Dario Amodei. Scaling laws for neural language
610 models. *CoRR*, abs/2001.08361, 2020. URL <https://arxiv.org/abs/2001.08361>.
611
- 612 Yuhang Li, Ruihao Gong, Xu Tan, Yang Yang, Peng Hu, Qi Zhang, Fengwei Yu, Wei Wang, and
613 Shi Gu. BRECQ: pushing the limit of post-training quantization by block reconstruction. In
614 *9th International Conference on Learning Representations, ICLR 2021, Virtual Event, Austria,*
615 *May 3-7, 2021*. OpenReview.net, 2021. URL [https://openreview.net/forum?id=](https://openreview.net/forum?id=POWv6hDd9XH)
616 [POWv6hDd9XH](https://openreview.net/forum?id=POWv6hDd9XH).
- 617 Ji Lin, Jiaming Tang, Haotian Tang, Shang Yang, Xingyu Dang, and Song Han. AWQ: activation-
618 aware weight quantization for LLM compression and acceleration. *CoRR*, abs/2306.00978, 2023.
619 doi: 10.48550/ARXIV.2306.00978. URL [https://doi.org/10.48550/arXiv.2306.](https://doi.org/10.48550/arXiv.2306.00978)
620 [00978](https://doi.org/10.48550/arXiv.2306.00978).
- 621 Zechun Liu, Barlas Oguz, Changsheng Zhao, Ernie Chang, Pierre Stock, Yashar Mehdad, Yangyang
622 Shi, Raghuraman Krishnamoorthi, and Vikas Chandra. LLM-QAT: data-free quantization aware
623 training for large language models. *CoRR*, abs/2305.17888, 2023. doi: 10.48550/ARXIV.2305.
624 17888. URL <https://doi.org/10.48550/arXiv.2305.17888>.
625
- 626 Zechun Liu, Changsheng Zhao, Igor Fedorov, Bilge Soran, Dhruv Choudhary, Raghuraman Krish-
627 namoorthi, Vikas Chandra, Yuandong Tian, and Tijmen Blankevoort. Spingquant: LLM quantiza-
628 tion with learned rotations. *CoRR*, abs/2405.16406, 2024a. doi: 10.48550/ARXIV.2405.16406.
629 URL <https://doi.org/10.48550/arXiv.2405.16406>.
- 630 Zirui Liu, Jiayi Yuan, Hongye Jin, Shaochen Zhong, Zhaozhuo Xu, Vladimir Braverman, Beidi
631 Chen, and Xia Hu. KIVI: A tuning-free asymmetric 2bit quantization for KV cache. In *Forty-first*
632 *International Conference on Machine Learning, ICML 2024, Vienna, Austria, July 21-27, 2024*.
633 OpenReview.net, 2024b. URL <https://openreview.net/forum?id=L057s2Rq8O>.
- 634 Harsh Mehta, Ankit Gupta, Ashok Cutkosky, and Behnam Neyshabur. Long range language mod-
635 eling via gated state spaces. In *The Eleventh International Conference on Learning Represen-*
636 *tations, ICLR 2023, Kigali, Rwanda, May 1-5, 2023*. OpenReview.net, 2023. URL [https://openreview.net/forum?id=](https://openreview.net/forum?id=5MkYIYCbva)
637 [5MkYIYCbva](https://openreview.net/forum?id=5MkYIYCbva).
638
- 639 Stephen Merity, Caiming Xiong, James Bradbury, and Richard Socher. Pointer sentinel mixture
640 models. In *5th International Conference on Learning Representations, ICLR 2017, Toulon,*
641 *France, April 24-26, 2017, Conference Track Proceedings*. OpenReview.net, 2017. URL [https://openreview.net/forum?id=](https://openreview.net/forum?id=Byj72udxe)
642 [Byj72udxe](https://openreview.net/forum?id=Byj72udxe).
- 643 Todor Mihaylov, Peter Clark, Tushar Khot, and Ashish Sabharwal. Can a suit of armor conduct
644 electricity? A new dataset for open book question answering. In Ellen Riloff, David Chiang,
645 Julia Hockenmaier, and Jun’ichi Tsujii (eds.), *Proceedings of the 2018 Conference on Empirical*
646 *Methods in Natural Language Processing, Brussels, Belgium, October 31 - November 4, 2018*,
647 pp. 2381–2391. Association for Computational Linguistics, 2018. doi: 10.18653/V1/D18-1260.
URL <https://doi.org/10.18653/v1/d18-1260>.

- 648 Markus Nagel, Rana Ali Amjad, Mart van Baalen, Christos Louizos, and Tijmen Blankevoort. Up
649 or down? adaptive rounding for post-training quantization. In *Proceedings of the 37th Inter-*
650 *national Conference on Machine Learning, ICML 2020, 13-18 July 2020, Virtual Event*, vol-
651 *ume 119 of Proceedings of Machine Learning Research*, pp. 7197–7206. PMLR, 2020. URL
652 <http://proceedings.mlr.press/v119/nagel20a.html>.
- 653 OpenAI. GPT-4 technical report. *CoRR*, abs/2303.08774, 2023. doi: 10.48550/ARXIV.2303.08774.
654 URL <https://doi.org/10.48550/arXiv.2303.08774>.
- 655 Kuntal Kumar Pal, Kazuaki Kashihara, Ujjwala Anantheswaran, Kirby C. Kuznia, Siddhesh Jagtap,
656 and Chitta Baral. Exploring the limits of transfer learning with unified model in the cybersecurity
657 domain. *CoRR*, abs/2302.10346, 2023. doi: 10.48550/ARXIV.2302.10346. URL <https://doi.org/10.48550/arXiv.2302.10346>.
- 660 Pratyush Patel, Esha Choukse, Chaojie Zhang, Aashaka Shah, Íñigo Goiri, Saeed Maleki, and Ri-
661 cardo Bianchini. Splitwise: Efficient generative LLM inference using phase splitting. In *51st*
662 *ACM/IEEE Annual International Symposium on Computer Architecture, ISCA 2024, Buenos*
663 *Aires, Argentina, June 29 - July 3, 2024*, pp. 118–132. IEEE, 2024. doi: 10.1109/ISCA59077.
664 2024.00019. URL <https://doi.org/10.1109/ISCA59077.2024.00019>.
- 665 Bo Peng, Eric Alcaide, Quentin Anthony, Alon Albalak, Samuel Arcadinho, Stella Biderman,
666 Huanqi Cao, Xin Cheng, Michael Chung, Leon Derczynski, Xingjian Du, Matteo Grella, Kran-
667 thi Kiran GV, Xuzheng He, Haowen Hou, Przemyslaw Kazienko, Jan Kocon, Jiaming Kong, Bart-
668 lomiej Koptyra, Hayden Lau, Jiaju Lin, Krishna Sri Ipsit Mantri, Ferdinand Mom, Atsushi Saito,
669 Guangyu Song, Xiangru Tang, Johan S. Wind, Stanislaw Wozniak, Zhenyuan Zhang, Qinghua
670 Zhou, Jian Zhu, and Rui-Jie Zhu. RWKV: reinventing rnns for the transformer era. In Houda
671 Bouamor, Juan Pino, and Kalika Bali (eds.), *Findings of the Association for Computational*
672 *Linguistics: EMNLP 2023, Singapore, December 6-10, 2023*, pp. 14048–14077. Association
673 for Computational Linguistics, 2023. doi: 10.18653/V1/2023.FINDINGS-EMNLP.936. URL
674 <https://doi.org/10.18653/v1/2023.findings-emnlp.936>.
- 675 Yanyuan Qiao, Zheng Yu, Longteng Guo, Sihan Chen, Zijia Zhao, Mingzhen Sun, Qi Wu, and Jing
676 Liu. VI-mamba: Exploring state space models for multimodal learning. *CoRR*, abs/2403.13600,
677 2024. doi: 10.48550/ARXIV.2403.13600. URL [https://doi.org/10.48550/arXiv.](https://doi.org/10.48550/arXiv.2403.13600)
678 [2403.13600](https://doi.org/10.48550/arXiv.2403.13600).
- 679 Keisuke Sakaguchi, Ronan Le Bras, Chandra Bhagavatula, and Yejin Choi. Winogrande: An ad-
680 versarial winograd schema challenge at scale. In *The Thirty-Fourth AAAI Conference on Artificial*
681 *Intelligence, AAAI 2020, The Thirty-Second Innovative Applications of Artificial Intelligence*
682 *Conference, IAAI 2020, The Tenth AAAI Symposium on Educational Advances in Artificial Intelli-*
683 *gence, EAAI 2020, New York, NY, USA, February 7-12, 2020*, pp. 8732–8740. AAAI Press, 2020.
684 doi: 10.1609/AAAI.V34I05.6399. URL [https://doi.org/10.1609/aaai.v34i05.](https://doi.org/10.1609/aaai.v34i05.6399)
685 [6399](https://doi.org/10.1609/aaai.v34i05.6399).
- 686 Jimmy T. H. Smith, Andrew Warrington, and Scott W. Linderman. Simplified state space lay-
687 ers for sequence modeling. In *The Eleventh International Conference on Learning Represen-*
688 *tations, ICLR 2023, Kigali, Rwanda, May 1-5, 2023*. OpenReview.net, 2023. URL <https://openreview.net/pdf?id=Ai8Hw3AXqks>.
- 690 Philippe Tillet, Hsiang-Tsung Kung, and David Cox. Triton: an intermediate language and compiler
691 for tiled neural network computations. In *Proceedings of the 3rd ACM SIGPLAN International*
692 *Workshop on Machine Learning and Programming Languages*, pp. 10–19, 2019.
- 693 Hugo Touvron, Thibaut Lavril, Gautier Izacard, Xavier Martinet, Marie-Anne Lachaux, Timothée
694 Lacroix, Baptiste Rozière, Naman Goyal, Eric Hambro, Faisal Azhar, Aurélien Rodriguez, Ar-
695 mand Joulin, Edouard Grave, and Guillaume Lample. Llama: Open and efficient foundation
696 language models. *CoRR*, abs/2302.13971, 2023. doi: 10.48550/ARXIV.2302.13971. URL
697 <https://doi.org/10.48550/arXiv.2302.13971>.
- 698 Ashish Vaswani, Noam Shazeer, Niki Parmar, Jakob Uszkoreit, Llion Jones, Aidan N. Gomez,
699 Lukasz Kaiser, and Illia Polosukhin. Attention is all you need. In Isabelle Guyon, Ulrike von
700 Luxburg, Samy Bengio, Hanna M. Wallach, Rob Fergus, S. V. N. Vishwanathan, and Roman
701

- 702 Garnett (eds.), *Advances in Neural Information Processing Systems 30: Annual Conference on*
703 *Neural Information Processing Systems 2017, December 4-9, 2017, Long Beach, CA, USA*, pp.
704 5998–6008, 2017. URL [https://proceedings.neurips.cc/paper/2017/hash/](https://proceedings.neurips.cc/paper/2017/hash/3f5ee243547dee91fbd053c1c4a845aa-Abstract.html)
705 [3f5ee243547dee91fbd053c1c4a845aa-Abstract.html](https://proceedings.neurips.cc/paper/2017/hash/3f5ee243547dee91fbd053c1c4a845aa-Abstract.html).
706
- 707 Roger Waleffe, Wonmin Byeon, Duncan Riach, Brandon Norick, Vijay Korthikanti, Tri Dao, Albert
708 Gu, Ali Hatamizadeh, Sudhakar Singh, Deepak Narayanan, Garvit Kulshreshtha, Vartika Singh,
709 Jared Casper, Jan Kautz, Mohammad Shoeybi, and Bryan Catanzaro. An empirical study of
710 mamba-based language models. *CoRR*, abs/2406.07887, 2024. doi: 10.48550/ARXIV.2406.
711 07887. URL <https://doi.org/10.48550/arXiv.2406.07887>.
- 712 Junxiong Wang, Jing Nathan Yan, Albert Gu, and Alexander M. Rush. Pretraining without at-
713 tention. In Houda Bouamor, Juan Pino, and Kalika Bali (eds.), *Findings of the Association for*
714 *Computational Linguistics: EMNLP 2023, Singapore, December 6-10, 2023*, pp. 58–69. Associ-
715 ation for Computational Linguistics, 2023. doi: 10.18653/V1/2023.FINDINGS-EMNLP.5. URL
716 <https://doi.org/10.18653/v1/2023.findings-emnlp.5>.
- 717 Xiuying Wei, Yunchen Zhang, Xiangguo Zhang, Ruihao Gong, Shanghang Zhang,
718 Qi Zhang, Fengwei Yu, and Xianglong Liu. Outlier suppression: Push-
719 ing the limit of low-bit transformer language models. In *NeurIPS*, 2022.
720 URL [http://papers.nips.cc/paper_files/paper/2022/hash/](http://papers.nips.cc/paper_files/paper/2022/hash/6f6db140de9c9f111b12ef8a216320a9-Abstract-Conference.html)
721 [6f6db140de9c9f111b12ef8a216320a9-Abstract-Conference.html](http://papers.nips.cc/paper_files/paper/2022/hash/6f6db140de9c9f111b12ef8a216320a9-Abstract-Conference.html).
- 722 Guangxuan Xiao, Ji Lin, Mickaël Seznec, Hao Wu, Julien Demouth, and Song Han. Smoothquant:
723 Accurate and efficient post-training quantization for large language models. In Andreas Krause,
724 Emma Brunskill, Kyunghyun Cho, Barbara Engelhardt, Sivan Sabato, and Jonathan Scarlett
725 (eds.), *International Conference on Machine Learning, ICML 2023, 23-29 July 2023, Honolulu,*
726 *Hawaii, USA*, volume 202 of *Proceedings of Machine Learning Research*, pp. 38087–38099.
727 PMLR, 2023. URL <https://proceedings.mlr.press/v202/xiao23c.html>.
728
- 729 Rowan Zellers, Ari Holtzman, Yonatan Bisk, Ali Farhadi, and Yejin Choi. Hellaswag: Can a ma-
730 chine really finish your sentence? In Anna Korhonen, David R. Traum, and Lluís Màrquez
731 (eds.), *Proceedings of the 57th Conference of the Association for Computational Linguistics,*
732 *ACL 2019, Florence, Italy, July 28- August 2, 2019, Volume 1: Long Papers*, pp. 4791–
733 4800. Association for Computational Linguistics, 2019. doi: 10.18653/V1/P19-1472. URL
734 <https://doi.org/10.18653/v1/p19-1472>.
- 735 Lianghui Zhu, Bencheng Liao, Qian Zhang, Xinlong Wang, Wenyu Liu, and Xinggang Wang. Vision
736 mamba: Efficient visual representation learning with bidirectional state space model. *CoRR*,
737 abs/2401.09417, 2024. doi: 10.48550/ARXIV.2401.09417. URL [https://doi.org/10.](https://doi.org/10.48550/arXiv.2401.09417)
738 [48550/arXiv.2401.09417](https://doi.org/10.48550/arXiv.2401.09417).
739
740
741
742
743
744
745
746
747
748
749
750
751
752
753
754
755

A APPENDIX

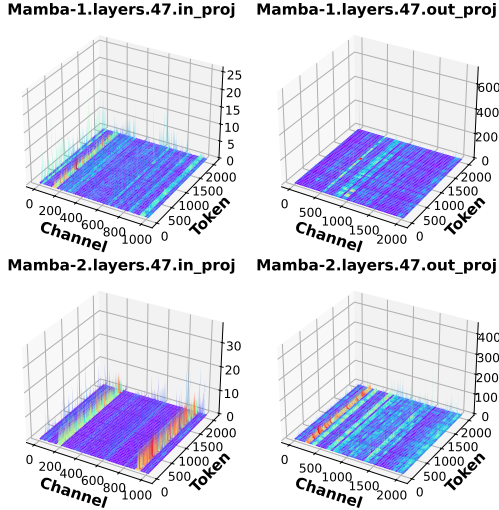


Figure 7: Visualization of inputs for linear projections. The out projection suffers from more severe outliers compared to the in projection.

A.1 PREVIOUS PTQ METHODS ON MAMBA

In Section 4, we analyze the quantization of linear projections in Mamba models. Here, we provide more detailed results about previous PTQ methods on Mamba-1 and Mamba-2 models. We will analyze the difference between Mamba-1 models and Mamba-2 models from a view of model quantization. The results presented in Table 6 indicate that Mamba2 models exhibit greater robustness to quantization compared to Mamba1 models. Further analysis in Figure 7 reveals that this improvement is largely due to the additional LayerNorm applied before the output projection in Mamba2, which helps to reduce outliers to a certain extent. Moreover, this LayerNorm simplifies the implementation of previous PTQ methods based on smoothing between weights and activations, such as SmoothQuant (Xiao et al., 2023) and AWQ (Lin et al., 2023). As a result, this paper primarily focuses on Mamba2 models, which not only feature larger state dimensions but are also more amenable to quantization.

Model	Method	WikiText2	C4
Mamba1-370M	FP	14.31	17.23
	W8A8	18.95	23.04
	W8A8+SQ	16.17	19.85
	W4A16+ GPTQ	16.03	19.06
Mamba2-370M	FP	14.16	16.95
	W8A8	17.14	20.10
	W8A8+SQ	15.71	18.72
	W4A16+GPTQ	15.81	18.71

Table 6: Different PTQ methods for Mamba models. Mamba-1 models suffer much more serious outliers in output projections because of the absence of LayerNorm before it.

A.2 PROOF

Theorem 2. Assuming $u_t \sim \mathcal{N}(\mathbf{0}, \sigma \mathbf{I}_n)$ and A_t is a constant, $B_t, x_t = \text{split}(W u_t)$ ($B_t \in \mathbb{R}^N$, $x_t \in \mathbb{R}^P$), the variance of states h_t can be factorized into two vectors:

$$h_t = A_t \cdot h_{t-1} + x_t \cdot B_t^\top \tag{15}$$

810
811
812
813
814
815
816
817
818
819
820
821
822
823
824
825
826
827
828
829
830
831
832
833
834
835
836
837
838
839
840
841
842
843
844
845
846
847
848
849
850
851
852
853
854
855
856
857
858
859
860
861
862
863

$$\text{Var}[h_t] \propto \alpha \cdot \beta^\top, \quad \alpha_i = \|W_{i,:}^x\|_2^2 \quad \text{and} \quad \beta_i = \|W_{i,:}^B\|_2^2 \quad (16)$$

where $\alpha \in \mathbb{R}^P$ and $\beta \in \mathbb{R}^N$ and $W^B, W^x = \text{split}(W, \text{dim} = 0)$

Proof. Firstly, we can reformulate Equation (??) as a prefix sum:

$$h_t = \sum_i^t A_{i:t} x_i B_i^\top, \quad \text{where} \quad A_{i:t} = A_i \times A_{i+1} \times \dots \times A_t \quad (17)$$

Then, we can compute the mean of states h_t as follows:

$$\begin{aligned} \mathbb{E}[h_t] &= \sum_i^t A_{i:t} \mathbb{E}[x_i B_i^\top] \\ &= \sum_i^t A_{i:t} \mathbb{E}[W^x u_i u_i^\top W^b{}^\top] \\ &= \sum_i^t A_{i:t} W^x \mathbb{E}[u_i u_i^\top] W^b{}^\top \\ &= \sum_i^t A_{i:t} \sigma W^x W^b{}^\top \end{aligned} \quad (18)$$

After computing the mean of the states, we can similarly compute the variance of the states h_t . The equality (a) is attributed to Lemma 1.

$$\begin{aligned} \text{Var}[x_i B_i^\top] &= \mathbb{E}[(W^x u_i u_i^\top W^b{}^\top - \sigma W^x W^b{}^\top)] \\ &= \mathbb{E}[(W^x (u_i u_i^\top) W^b{}^\top)^2] - 2\sigma \cdot \mathbb{E}[W^x W^b{}^\top \odot (W^x u_i u_i^\top W^b{}^\top)] + (\sigma W^x W^b{}^\top)^2 \\ &\stackrel{(a)}{=} \sigma^2 \alpha \cdot \beta^\top + 2\sigma^2 \cdot (W^x W_b^\top)^2 - 2\sigma^2 \cdot (W^x W_b^\top)^2 + \sigma^2 \cdot (W^x W^b{}^\top)^2 \\ &= \sigma^2 \alpha \cdot \beta^\top + \sigma^2 \cdot (W^x W^b{}^\top)^2 \end{aligned} \quad (19)$$

Here, we assume that the second term $(W^x W^b{}^\top)^2$ is sufficiently small compared to $\alpha \cdot \beta^\top$, and then we obtain:

$$\text{Var}[h_t] = (\sigma^2 \sum_i^t A_{i:t}) \cdot (\alpha \cdot \beta^\top) \quad (20)$$

□

Lemma 1. Assuming $z \sim \mathcal{N}(\mathbf{0}, \mathbf{I}_n)$, $w_1, w_2 \in \mathbb{R}^n$, we have the following conclusions:

$$\mathbb{E}[(w_1^\top z)^2 (w_2^\top z)^2] = \|w_1\|_2^2 \cdot \|w_2\|_2^2 + 2(w_1^\top w_2)^2 \quad (21)$$

864
865
866
867
868
869
870
871
872
873
874
875
876
877
878
879
880
881
882
883
884
885
886
887
888
889
890
891
892
893
894
895
896
897
898
899
900
901
902
903
904
905
906
907
908
909
910
911
912
913
914
915
916
917

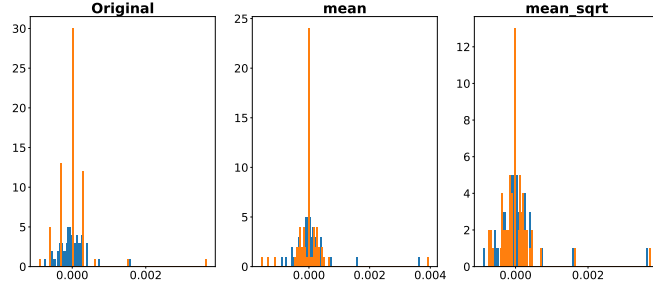


Figure 8: An illustration of how DSQ enhances performance.

Proof. Let A and B be two arbitrary symmetric matrices, we have:

$$\begin{aligned}
 \mathbb{E}[x^\top Ax \cdot x^\top Bx] &= \mathbb{E}\left[\sum_{i,j} x_i a_{ij} x_j \sum_{k,l} x_k b_{kl} x_l\right] \\
 &= \mathbb{E}\left[\sum_{i,k} a_{ii} b_{kk} x_i^2 x_k^2 + 4 \sum_{i<j} a_{ij} b_{ij} x_i^2 x_j^2\right] \\
 &= \sum_{i,k} a_{ii} b_{kk} + 2 \sum_i a_{ii} b_{ii} + 2 \left(\sum_{i,j} a_{ij} b_{ij} - \sum_i a_{ii} b_{ii}\right) \\
 &= \sum_i a_{ii} \sum_k b_{kk} + 2 \sum_{i,j} a_{ij} b_{ij} \\
 &= \text{Tr}(A)\text{Tr}(B) + 2\text{Tr}(AB)
 \end{aligned} \tag{22}$$

A special case occurs when $A = w_1 w_1^\top$ and $B = w_2 w_2^\top$:

$$\mathbb{E}[(w_1^\top z)^2 (w_2^\top z)^2] = \|w_1\|_2^2 \cdot \|w_2\|_2^2 + 2(w_1^\top w_2)^2 \tag{23}$$

□

Although this theorem imposes strict constraints on the SSM inputs u_t (Gaussian distribution) and A_t (constant), it sufficiently reveals the following fact: outliers in the channel dimension P and state dimension N can be attributed to the variables $x_t \in \mathbb{R}^{(T,P)}$ and $B_t \in \mathbb{R}^{(T,N)}$, respectively. Figure 3 provides a visualization of this phenomenon.

A.3 MORE ABLATION STUDIES

Visualization of DSQ. Figure 8 illustrates how DSQ improves performance. The presence of outliers causes MinMax quantization to waste a significant portion of available quantization slots, resulting in large rounding errors. Although introducing channel scales $S_{channel}$ helps make the quantization slots non-uniform, the mean norm remains sensitive to outliers, even unexpectedly amplifying them (as shown in the middle figure).

Trainable parameters in ESR. Table 7 demonstrates the effectiveness of our choice of trainable parameters in ESR: Fine-tuning selective parameters (B , C , and Δ), layer normalization, and convolution yields the best perplexity. In contrast, including x and z results in worse performance. We attribute this to the fact that fine-tuning all parameters can lead to overfitting and necessitates end-to-end training.

A.4 PSEUDOCODE

In this section, we present the pseudocode for the parallel training of quantization-aware SSMs. To enhance understanding, we also include the pseudocode for the recurrent and quadratic modes of

	Norm	Δ, B, C, D	Conv-1D	X, Z	WikiText2	C4
918					25.73	29.94
919					24.76	29.02
920	✓				23.27	27.22
921		✓			25.24	29.09
922			✓		24.99	28.88
923				✓	22.51	27.00
924	✓	✓			24.93	28.87
925	✓		✓		25.31	29.43
926	✓			✓	22.68	26.91
927		✓	✓		22.97	26.41
928		✓		✓	25.66	28.89
929			✓	✓	21.92	25.99
930	✓	✓			23.63	27.43
931	✓		✓	✓	24.89	29.04
932		✓	✓	✓	23.01	26.98
933	✓	✓	✓	✓	23.73	28.19

Table 7: The performance of W16A16H4 quantization for Mamba2-370M with different trainable parameters in the ESR.

Mamba-2. It is worth noting that these pseudocodes are provided solely for illustrative purposes and do not represent actual implementations.

```

941
942 1 def ParallelSSM(
943 2     A, # bsz * num_head * len
944 3     B, # bsz * num_head * len * state_dim
945 4     C, # bsz * num_head * len * state_dim
946 5     x # bsz * num_head * len * channel_dim
947 6 ):
948 7     BC = C @ B.transpose(-1, -2)
949 8     prefix_sum = torch.cumsum(A)
950 9
951 10     # L : bsz * num_head * len * len
952 11     L = torch.tril(prefix_sum.unsqueeze(-1) - prefix_sum.unsqueeze(-2))
953 12
954 13     ABC = L * BC
955 14     y = ABC @ x
956 15     return y
957
958 1 def RecurrentSSM_onestep(
959 2     A, # bsz * num_head
960 3     B, # bsz * num_head * state_dim
961 4     C, # bsz * num_head * state_dim
962 5     x, # bsz * num_head * channel_dim
963 6     last_state # bsz * num_head * channel_dim * state_dim
964 7 ):
965 8     current_state = A * last_state + B.unsqueeze(-2) * x.unsqueeze(-1)
966 9     output = current_state @ C.unsqueeze(-1)
967 10     return output.squeeze(-1)
968
969 1 def QuantizationAwareParallelSSM(
970 2     A, # bsz * num_head * len
971 3     B, # bsz * num_head * len * state_dim
972 4     C, # bsz * num_head * len * state_dim
973 5     x # bsz * num_head * len * channel_dim
974 6 ):
975 7     BX = B.unsqueeze(-2) * x.unsqueeze(-1)
976 8     prefix_sum = torch.cumsum(A)

```

```
972 9 L = torch.tril(prefix_sum.unsqueeze(-1) - prefix_sum.unsqueeze(-2))
973 10 state = torch.einsum('bh1dn,bh1l->bh1dn', BX, L)
974 11
975 12 # Simulate the quantization errors at the last timestep
976 13 # Error case: qstate = fake_quant(state)
977 14 qstate = A[:, :, 1:] * fake_quant(state)[:, :, :-1] + BX[:, :, 1:]
978 15
979 16 y = torch.einsum('bh1dn,bh1n->bh1d', qstate, C)
980 17 return y
981
982
983
984
985
986
987
988
989
990
991
992
993
994
995
996
997
998
999
1000
1001
1002
1003
1004
1005
1006
1007
1008
1009
1010
1011
1012
1013
1014
1015
1016
1017
1018
1019
1020
1021
1022
1023
1024
1025
```